Spectral and spatial investigation of midinfrared surface waves on a plasmonic grating

T. Ribaudo,[1] D. C. Adams,[1] B. Passmore,[2] E. A. Shaner,[2] and D. Wasserman[1,a)]
[1]*Department of Physics and Applied Physics, University of Massachusetts Lowell, Lowell, Massachusetts 01854, USA*
[2]*Sandia National Labs, P.O. Box 5800, Albuquerque, New Mexico 87185, USA*

(Received 5 March 2009; accepted 30 April 2009; published online 21 May 2009)

A patterned metal film with a periodic array of subwavelength apertures, fabricated upon a semiconductor substrate and designed to possess transmission resonances in the midinfrared is interrogated with a wavelength-tunable external cavity quantum cascade laser. The interaction of the coherent light with this plasmonic structure is studied using a spatially resolved transmission experiment, allowing for the far-field imaging of propagating waves on the surface of the metal film. Spatial and spectral transmission is investigated for a range of near-normal incidence angles. For nonzero angles of incidence, coupling of laser light, at distinct frequencies, to surface waves propagating in opposite directions is demonstrated. © *2009 American Institute of Physics*.
[DOI: 10.1063/1.3140569]

Significant attention has been given, of late, to the unique optical properties associated with periodic arrays of subwavelength apertures[1] or subwavelength slits[2] in metallic films. Many of the phenomena under investigation are argued to be a result of surface plasmon (SP) excitations at the interface between the patterned metal films and the surrounding dielectric material. These plasmonic structures hold potential for the development of novel technologies in display,[3] sensing,[4] beam steering,[5] and on-chip communication or interconnect applications.[6]

For on-chip interconnect or sensing applications, the ability to control the propagation direction of a surface excitation would be quite useful. Recently we have demonstrated the ability to modulate the coupling of incident laser light to propagating surface waves on a plasmonic structure known as an extraordinary optical transmission (EOT) grating.[1] By actively controlling the optical properties of the EOT grating, we were able to both control coupling to waves on the plasmonic surface, and image the resulting surface waves using a far-field measurement technique.[7] This work demonstrated a spectral separation between the resonant transmission peak of the EOT grating and the wavelength for which maximum propagation lengths were observed. However, due to the limited tuning range of the plasmonic structure, a full picture of the interaction between coherent radiation and the plasmonic surface was not realized. In this work, we use a passive plasmonic structure, which we interrogate using a Daylight Solutions Inc. tunable external cavity quantum cascade laser (ECQCL). By investigating the interaction of the coherent midinfrared (mid-IR) light incident upon the EOT grating as a function of wavelength, for a range of angles, we are able to image the propagating surface waves and study the coupling to these waves as a function of the structure's transmission spectra.

The initial explanations of the EOT phenomenon suggested the resonant transmission to be a result of incident light coupling to SP polaritons (SPPs) at the metal/dielectric interface. Recent work has demonstrated microscopic theories for EOT transmission, which reinforce the role of SPPs in this process,[8,9] In these works, the extraordinary transmission effect is demonstrated to be a result of incident radiation coupling to, constructively or destructively interfering with, and scattering from surface modes. However, an additional surface wave, referred to as a quasi-cylindrical wave (CW) is required to fully explain the phenomenon. These microscopic theories focus on the visible/near-IR spectral range, and, at least in the case of Ref. 8, do note that the EOT mechanisms at longer wavelengths could be markedly different from those at shorter wavelengths, a result supported by earlier work in the terahertz frequency range.[10] Specifically, at longer wavelengths, coupling to the SPP modes is much weaker, and the CW could play a more dominant role in the EOT process. While the results presented here are not able to differentiate between CW and SPPs on our sample surface, a measure of the long-range propagation as a function of spectral position on the device transmission spectrum could serve to illuminate the mid-IR EOT process for future experimental and theoretical work.

The sample studied in this work consisted of a metal film with a periodic array of subwavelength apertures deposited upon an epi-ready semi-insulating GaAs wafer. A square lattice of 1.5 μm apertures, with a periodicity of 3.05 μm, was patterned in the metal film by standard UV photolithography, followed by a 60 nm Au metallization and lift-off process. The expression for the SPP resonance, for normally incident radiation, of this EOT grating is given by

$$\sqrt{i^2+j^2}\lambda_{\mathrm{SPP}} = a_o\sqrt{\frac{\varepsilon_s\varepsilon_m}{\varepsilon_s+\varepsilon_m}} \approx a_o\sqrt{\varepsilon_s} \quad \text{for} \quad |\varepsilon_m| \gg |\varepsilon_s|. \quad (1)$$

Here, λ_{SPP} is the SPP wavelength, a_o is the lattice constant of the aperture array, i and j are integers related to the grating reciprocal lattice vectors $2\pi/a_o\,\hat{\mathbf{x}}$ and $2\pi/a_o\,\hat{\mathbf{y}}$ respectively, ε_s is the real part of the dielectric constant of the semiconductor, and ε_m is the real part of the dielectric constant of the metal. In the mid-IR, $|\varepsilon_m| \gg |\varepsilon_s|$ for the metals typically used in EOT devices (Au, Cu, Ag, and Al), which allows Eq. (1) to be reduced to its simplified form.

a)Electronic mail: daniel_wasserman@uml.edu.

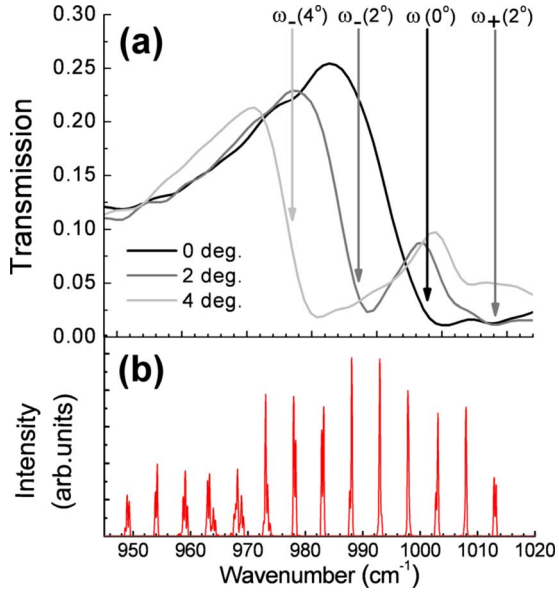

FIG. 1. (Color online) (a) Broadband transmission through EOT grating for incidence angles of 0°, 2°, and 4° with predicted spectral position of resonant coupling to SPPs noted for each angle. (b) ECQCL emission for selected wavelengths across the laser's tunable range.

Equation (1) gives the resonant SPP wavelength for light normally incident upon a square lattice array of apertures in a metal film deposited upon a semiconductor. In this case, the incident photon carries no in-plane momentum ($k_x=0$), and an incident photon with wavelength λ_{SPP} can couple to SPPs propagating in both the $+x$ and $-x$ directions. However, as the angle of incidence increases, the degeneracy of the $(+1,0)$ and $(-1,0)$ SPP modes is lifted. The lifting of this degeneracy is typically seen in a splitting of the resonant transmission peaks for an EOT grating.[11] What is not immediately obvious from the spectral data, however, is that the two split peaks each represent SPP modes propagating in opposite directions. Equation (2) gives the resonant SPP frequencies for non-normal incidence excitation of an EOT grating:

$$\omega_{\pm} = \frac{2\pi c}{a_o}\left(\sqrt{\frac{\varepsilon_s \varepsilon_m}{\varepsilon_s + \varepsilon_m}} \mp \sqrt{\varepsilon_s}\sin\theta\right)^{-1}. \quad (2)$$

Here ω_+ corresponds to the frequency of light coupling to the forward propagating $(+x)$ SPP, while ω_- corresponds to the frequency of light coupling to the backward propagating $(-x)$ SPP. By varying the wavelength of the incident radiation, coupling to surface waves propagating in both the $+x$ and $-x$ directions should be achievable.

The broadband transmission of the EOT grating is first studied as a function of incidence angle. The horizontally (x) polarized broadband mid-IR source of a Bruker Vertex70 Fourier Transform Infrared spectrometer was focused onto the sample with a 200 mm focal length lens through a wire grid polarizer. The sample was rotated about the vertical axis, thereby altering the in-plane component of the incident photons' momentum in the x-direction only. Figure 1(a) shows the transmission spectra of the EOT grating for incidence angles of 0°, 2°, and 4°, and the predicted ω_{SPP}'s for each from Eq. (2), which are positioned at or near the minimum of each spectrum's Fano line shape. Figure 1(b) displays selected emission spectra across the tuning range of the ECQCL.

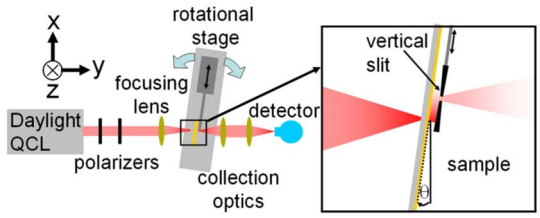

FIG. 2. (Color online) Schematic of the experimental setup for study of spatially and spectrally resolved transmission of ECQCL emission through an EOT grating as a function of incidence angle.

Following the initial characterization of both the sample and the ECQCL, the propagation of surface waves on the EOT structure is measured using the spatial and spectral characterization setup shown schematically in Fig. 2. Emission from the pulsed Daylight Solutions laser passes through two polarizers, the first is fixed to 45°, while the second can be switched between 0° and 90°, corresponding to horizontally (x) and vertically (y) polarized light. The laser emission is then focused onto the EOT surface, through the GaAs substrate. A vertical slit (10 μm) is attached to a translational stage, and aligned to travel across the metal surface of the sample in the x-direction. Both the sample and the translational stage are mounted on an automated rotational stage, which rotates around the focal point of the laser light on the sample. The transmitted laser light is recollimated and focused onto an external HgCdTe detector, which feeds into a lock-in amplifier (LIA). The LIA signal is then collected by the same software which controls the sample rotation and slit position. It should be noted that these are far-field measurements with the slit positioned approximately 100 μm away from the sample surface. In addition, it is the long propagation lengths of mid-IR plasmons (hundreds of microns), which allows for the use of this technique, as we can spatially distinguish between the directly transmitted laser light and the light scattered out after coupling to propagating SPPs. Initial data is collected with no sample in the beam path, allowing for a determination of the laser focal point, as well as the wavelength-dependent emission power of the laser, which is used to normalize the scans collected for each wavelength to the laser power at that wavelength. The sample is then placed in the beam path, and for each wavelength, the slit is scanned across the sample, providing a profile of transmitted/scattered light at the sample surface. The experiment was repeated for incident angles from −5° to 5°, in 1° increments, for both vertically and horizontally polarized light.

Figure 3 shows the resulting data from the experiments conducted. For the data displayed, each spatial scan for a given wavelength was normalized from zero to one. Though this does not give an accurate picture of total transmission (which is shown for each horizontally polarized data set with the overlaid broadband transmission spectra), it allows for better viewing of the propagating modes. Figures 3(a) and 3(b) show normally incident laser light of horizontal and vertical polarizations, respectively. For lower energies (<985 cm^{-1}), narrow Gaussian spatial profiles with full width at half maximum between 80–85 μm are observed on the sample surface, for both polarizations. However, at

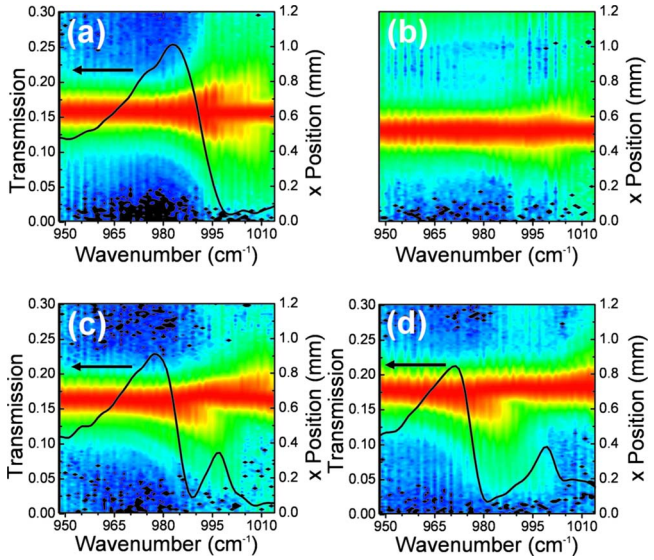

FIG. 3. (Color online) Contour plot of transmitted/scattered light intensity as a function of position and wavelength for (a) horizontally and (b) vertically polarized normally incident radiation. Contour plots for horizontally polarized laser incident at (c) 2° and (d) 4°. For all plots, the spatial scan for each laser wavelength is normalized from zero to one, to better image propagation. Broadband EOT transmission spectra for incidence angles of 0°, 2°, and 4° are overlaid on plot (a), (c), and (d), respectively.

higher energies, beginning near the peak of the EOT spectrum, the spatial profile of the horizontally polarized light begins to symmetrically broaden, an effect which we attribute to the coupling of the incident laser light to the degenerate $(\pm 1,0)$ SPP modes. In the vertical polarization, shown in Fig. 3(b), no such broadening is observed, as light polarized in the *y*-direction should not efficiently couple to horizontally propagating SPPs. Figure 3(c) shows the spatial profile of the transmitted/scattered light as a function of laser wavelength for an incidence angle of 2°. Here we can see the splitting of the $(-1,0)$ and $(+1,0)$ SPP modes, as the spatial profile of the beam first extends predominantly in the $-x$ and then, as the laser frequency is increased, to the $+x$ direction. This splitting grows more pronounced as the incidence angle increases to 4° [Fig. 3(d)]. At 4°, the splitting of the modes is large enough to push the spectral position of the $(+1,0)$ SPP mode past the range of the tunable laser.

From the data in Fig. 3, it can be seen that the propagation maximum, for each angle of incidence, is spectrally distinct from the EOT spectral peak. For all angles studied, the propagation maximum lies at, or near, the transmission minimum, which is also the calculated spectral position of the resonant coupling to the SPP for the given experimental configuration. Such a result is not unexpected, as the transmission maximum depends not only on the coupling to the surface waves, but also on the interference between these waves with the directly transmitted light, which results in maximized transmission at longer wavelengths then the SPP wavelength.[8]

In conclusion, by using a wavelength tunable ECQCL with a spatially resolved transmission experiment, we are able to recover far-field images of propagating surface modes on patterned metal/dielectric surfaces. By varying the laser angle of incidence we are able to break the degeneracy of the $(+1,0)$ and $(-1,0)$ surface modes, and image the propagation of these modes in opposite directions. These results provide a more complete picture of the mid-IR EOT process and could be utilized in the design and fabrication of a new class of plasmonic routing or switching devices for optical interconnect or on-chip sensing applications.

The authors would like to thank C. Gmachl and the NSF-ERC Mid-Infrared Technology for Health and the Environment (MIRTHE), for use of the Daylight Solutions tunable laser. Sandia is a multiprogram laboratory operated by Sandia Corporation, a Lockheed Martin Co., for the United States Department of Energy's National Nuclear Security Administration under Contract No. DE-AC04-94AL85000.

[1] T. W. Ebbesen, H. J. Lezec, H. F. Ghaemi, T. Thio, and P. A. Wolff, Nature (London) **391**, 667 (1998).
[2] D. Pacifici, H. J. Lezec, H. A. Atwater, and J. Weiner, Phys. Rev. B **77**, 115411 (2008).
[3] C. Genet and T. W. Ebbesen, Nature (London) **445**, 39 (2007).
[4] K. R. Rodriguez, S. Shah, S. M. Williams, S. Teeters-Kennedy, and J. V. Coe, J. Chem. Phys. **121**, 8671 (2004).
[5] L. Martín-Moreno, F. J. García-Vidal, H. J. Lezec, A. Degiron, and T. W. Ebbesen, Phys. Rev. Lett. **90**, 167401 (2003).
[6] J. T. Kim, J. J. Ju, S. Park, M. Kim, S. K. Park, and M.-H. Lee, Opt. Express **16**, 13133 (2008).
[7] T. Ribaudo, E. A. Shaner, S. S. Howard, C. Gmachl, X. J. Wang, F.-S. Choa, and D. Wasserman, Opt. Express **17**, 7019 (2009).
[8] H. Liu and P. Lalanne, Nature **452**, 728 (2008).
[9] D. Pacifici, H. J. Lezec, L. A. Sweatlock, R. J. Walters, and H. A. Atwater, Opt. Express **16**, 9222 (2008).
[10] J. B. Pendry, L. Martín-Moreno, and F. J. Garcia-Vidal, Science **305**, 847 (2004).
[11] H. F. Ghaemi, T. Thio, D. E. Grupp, T. W. Ebbesen, and H. J. Lezec, Phys. Rev. B **58**, 6779 (1998).